Cloud-Resolving Model Simulation and Mosaic Treatment of Subgrid Cloud-Radiation Interaction

X. Wu
Department of Geological and Atmospheric Sciences
Iowa State University
Ames, Iowa

X.-Z. Liang
Illinois State Water Survey
University of Illinois at Urbana-Champaign
Champaign, Illinois

Introduction

Improving the representation of cloud-radiation interaction is a major challenge for the global climate simulation. The development of cloud-resolving models (CRMs) and the extensive Atmospheric Radiation Measurements (ARMs) provide a unique opportunity for shading some lights on this problem. Current general circulation models (GCMs) predict cloud cover fractions and hydrometeor concentrations only in individual model layers, where clouds are assumed to be horizontally homogeneous in a coarse grid. They do not explicitly specify geometric associations or optical variations. Subsequently, clouds within a GCM grid are represented as a single effective volume that impacts radiation using various overlap assumptions (Liang and Wang 1997). On the other hand, the CRMs explicitly resolve convection and mesoscale organization, where cloud microphysical processes and cloud-radiation interactions directly respond to the cloud-scale dynamics (Grabowski et al. 1996, Wu et al. 1999, Wu and Moncrieff 2001). In particular, the fine spatial resolution allows the CRM to more realistically represent the detailed structure of cloud systems, including cloud geometric and radiative properties. The CRM simulations in combination with the ARM measurements thus provide comprehensive datasets, based on which a more realistic GCM parameterization of sub-grid cloud-radiation interactions can be developed.

The objective of our research project is to apply longterm CRM simulations to develop robust cloud statistics on subgrid cloud-radiation interactions and subsequently improve the GCM parameterization of these interactions using a mosaic treatment. This will contribute to the fundamental goal of the ARM program to improve the treatment of radiation and clouds in GCMs used to predict future climate. Our strategy is to first evaluate CRM simulations against ARM measurements, then quantify subgrid cloud variability, and finally improve GCM cloud-radiation parameterizations.

CRM Simulations and Evaluations with ARM Measurements

The CRM (Wu et al. 1999) is an improved version of the Clark-Hall model, which is based on a finite-difference formulation of the anelastic and nonhydrostatic equations (Clark et al. 1996). In particular,

we have incorporated an interactive cloud-radiation scheme based on the National Center for Atmospheric Research (NCAR) Community Climate Model Version 3 (CCM3; Kiehl et al. 1996). This facilitates direct intercomparisons between ARM measurements, CCM3-based single column model (SCM) calculations, and CRM simulations. The research findings will thus be readily transferable to improve parameterizations in GCMs (CCM3 in this case).

The CRM adopts a two-dimensional (2D) domain with a 600 km east-west width at 3-km grid spacing and a 40 km column of 51 vertical layers of stretched thicknesses ranging from 100 m at the surface to 1500 m at the model top. Periodic lateral boundary conditions are employed (Grabowski et al. 1996), while time-varying large-scale forcings are taken from the ARM constrained variational analysis (Zhang and Lin 1997). A 26-day (June 22 to July 17) CRM integration during the ARM 1997 intensive operational period (IOP) was conducted, where the large-scale forcings were provided by Shaocheng Xie at the Lawrence Livermore National Laboratory. We added a random perturbation with the amplitude of 0.5 K in the temperature field below 3 km to remedy the unrealistic buildup of moisture and energy (causing excessive rainfall) during the passage of cold fronts (especially in July 3-4). Due to the lack of surface moisture measurement, the CRM was forced with concurrent ARM observations of surface latent and sensible heat flux.

Wu and Liang (2003) compared the CRM simulations with the concurrent ARM measurements. The CRM realistically reproduces precipitation evolutions observed during the IOP. The cloud liquid water content compares reasonably well with the ARM measurements. More importantly, the CRM simulates both longwave (LW) and shortwave (SW) radiative fluxes at the surface and the top of atmosphere (TOA) that, when averaged in the entire IOP, simultaneously agree with observations within the measurement uncertainty. This result, consistent with our previous finding based on the Tropical Ocean Global Atmosphere-Coupled Ocean Atmosphere Response Experiment (TOGA-COARE) simulations (Wu and Moncrieff 2001), demonstrates that the CRM is capable of faithful representation of cloud-radiation interactions over both land and ocean. Figure 1 depicts the correspondence between observed and simulated daily mean radiative fluxes. The observed surface SW radiative fluxes were estimated by Li et al. (1993), while the TOA LW and SW fluxes were retrieved by Patrick Minnis of National Aeronautics and Space Administration (NASA) Langley Research Center. The result further indicates that the CRM correctly captures temporal variations of cloud-radiation interactions.

Given its credibility in reproducing the ARM measurements, the CRM can be applied to conduct sensitivity experiments to quantify relative contributions of various GCM simplifications on cloud-radiation interactions. Figure 2 illustrates how to construct, from the CRM outputs (M0), appropriate distributions of cloud properties that duplicate a typical GCM approach (M1) or remove inhomogeneity effect (M2). In M0, the radiation calculation is performed at each column assuming binary clouds (i.e., completely overcast or clear skies) at individual layers and the average over all 200 columns represents the bulk value at the GCM grid. The M2 is similar to the M0 except that the cloud prosperities at each overcast layer in individual columns are replaced by the domain-averaged value at that layer. In contrast, the radiation calculation in M1 is done only once from the domain-averaged profiles of cloud radiative properties and cloud fractions assuming that individual cloudy layers are randomly overlapped.

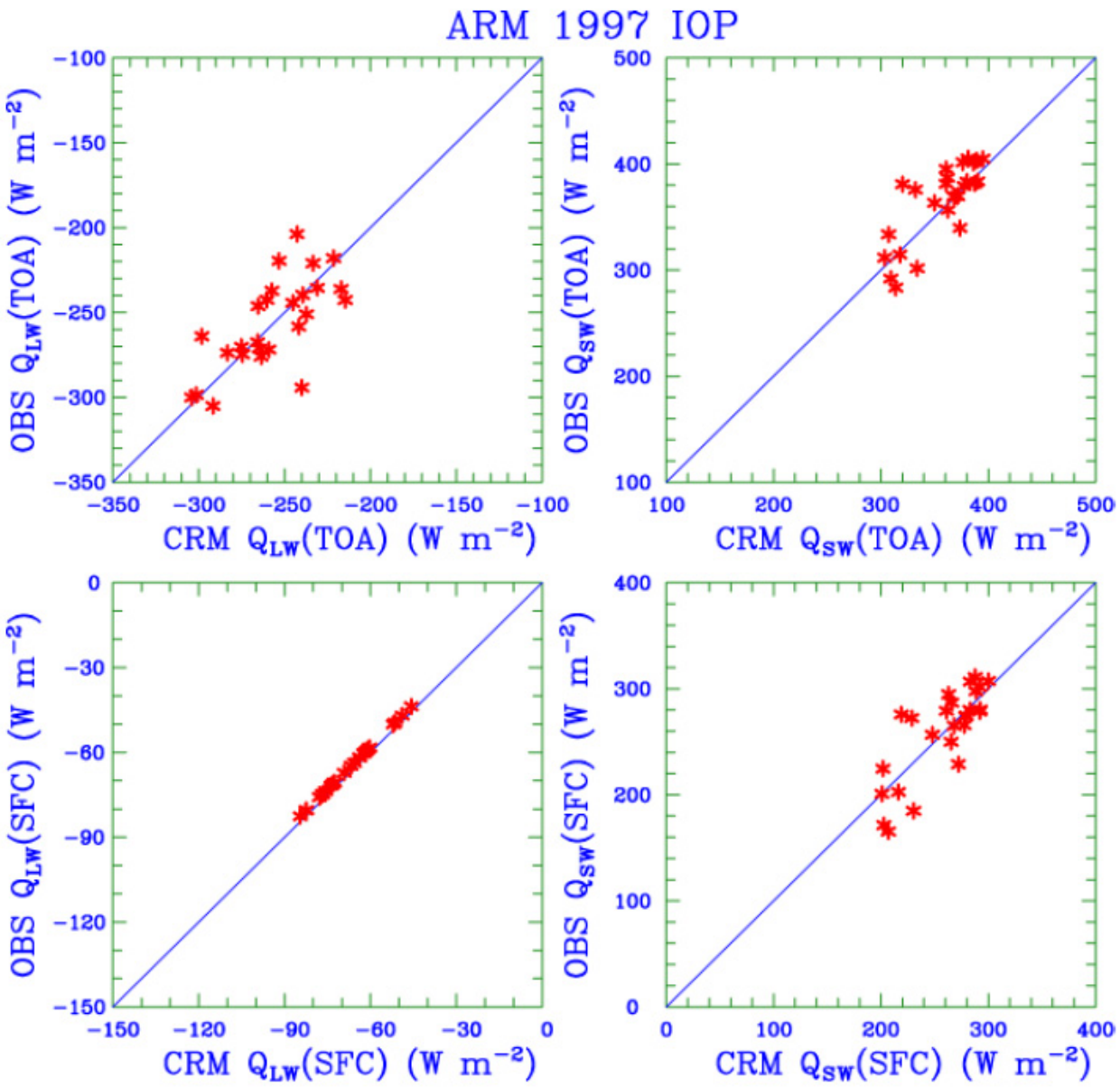

Figure 1. Scatter diagrams between observed (OBS) and simulated (CRM) daily mean LW (Q_{LW}) and SW (Q_{SW}) net fluxes (W m^{-2}) at the surface (SFC) and TOA. Downward fluxes are positive.

Figure 3 compares surface and TOA radiative fluxes with all 15-minute samples between the three approaches, where the M0 versus M2 shows the cloud inhomogeneity effect, while M2 versus M1 depicts the cloud geometry effect. Clearly the cloud inhomogeneity and geometry effects are equally important and generally additive (i.e., having a same sign of increase or decrease). The geometry (inhomogeneity) effect causes larger incoming solar radiation or outgoing LW radiation in low-medium (higher) ranges. Although the effects on SW and LW radiative heating of the atmosphere-surface system are generally opposite, they are not totally canceled out, with net cloud-radiative forcings.

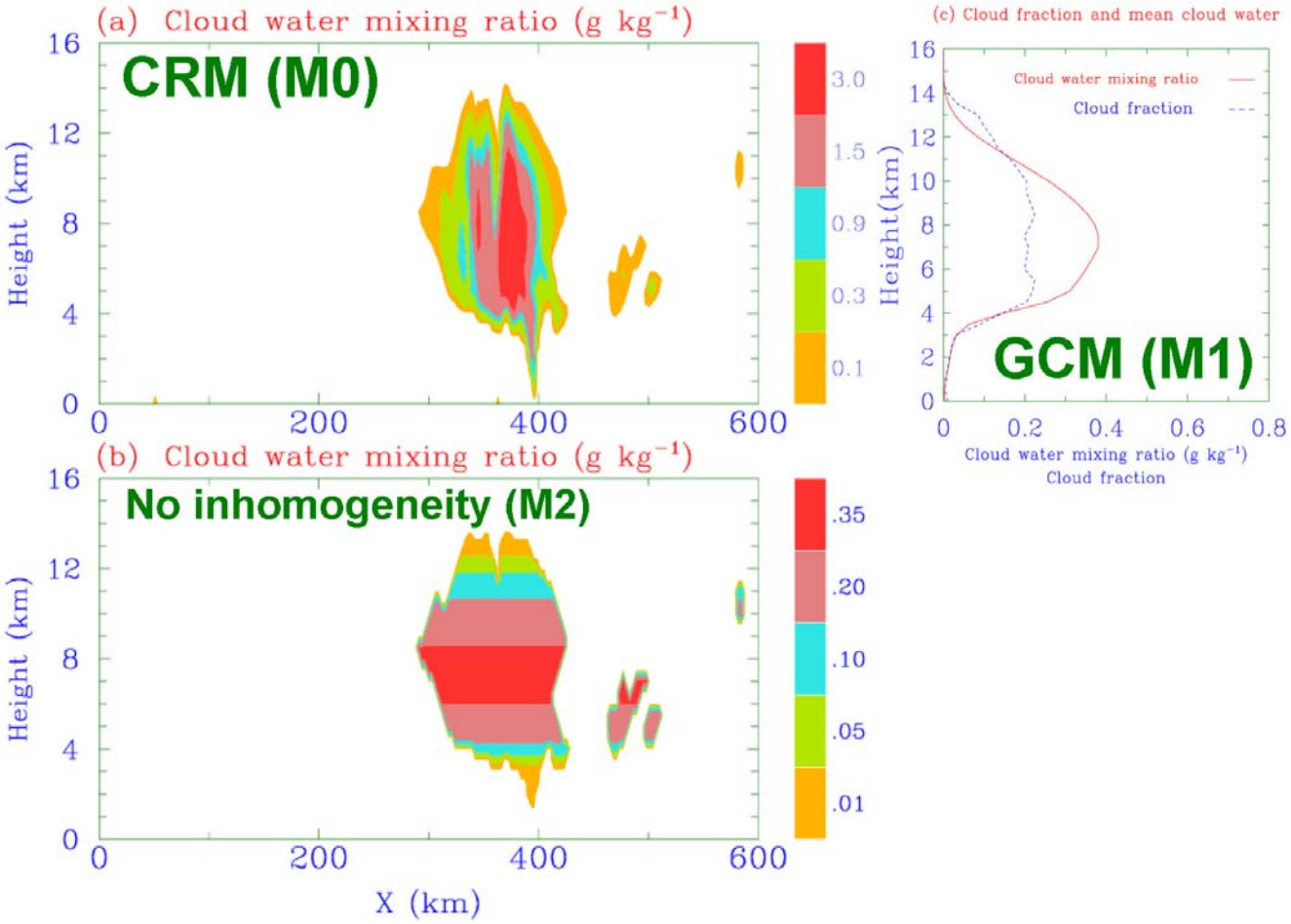

Figure 2. A CRM output sample of cloud water mixing ration (g kg^{-1}) distribution (a) and illustrations of how the horizontal inhomogeneity effect is removed (b) and the GCM calculation is formulated(c).

Mosaic Treatment of Subgrid Cloud-Radiation Interaction

Liang and Wang (1997) developed a mosaic treatment to cost-effectively incorporate subgrid cloud-radiation interactions into a GCM. The treatment divides the GCM grid into multiple subcells so that an individual layer within the subcell is either completely overcast or cloud free. Each overcast subcell layer contains a specific cloud genus with distinct optical properties. The most important consideration is to distinguish, within individual cloudy subcells, two cloud fractions: one with and another without inherent geometric association. In particular, convective (Cc), anvil cirrus (Ci) and stratiform (Cs) clouds in each layer are defined to be geographically distinct and thus minimally overlapped; Cc are assigned to a single subcell column, while Ci fill consecutively the remaining subcells; Cs is distributed into random-ordered subcells with an identical sequence for adjacent layers (maximum overlap) and otherwise independent sets for random overlap. Separate radiation calculations are then performed for each subcell with clouds, whereas clear-sky radiative properties and fluxes are computed only once and used for all subcells when needed. The grid mean radiative heating/cooling distributions are then the area averages over all subcells. Consequently, this mosaic treatment can adequately address the cloud

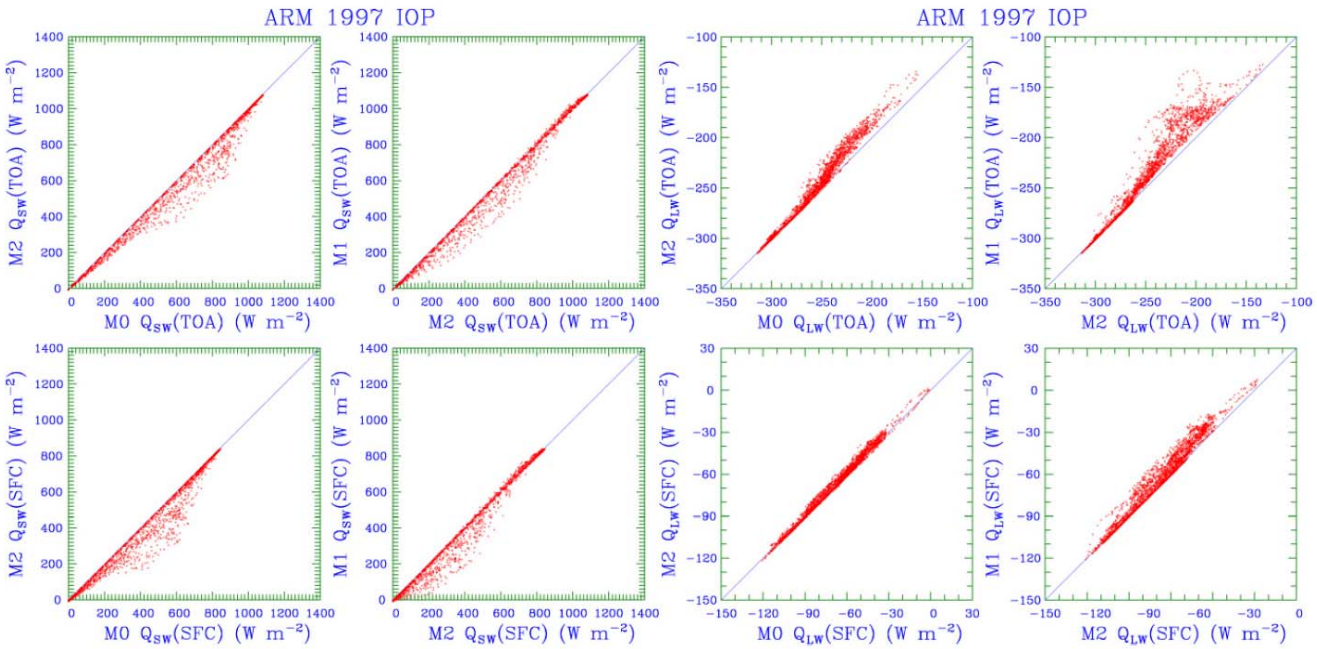

Figure 3. Scatter diagrams of M0 versus M2 (cloud inhomogeneity effect) and M2 versus M1 (cloud geometry effect) for LW (Q_{LW}) and SW (Q_{SW}) net fluxes (W m^{-2}) at the surface (SFC) and TOA. Downward fluxes are positive and all 15-minute samples are included.

macrogrouping (geometric association) and inhomogeneity (within-cloud optical property variance) effects on radiation.

Although the mosaic treatment is physically intuitive and results in improved GCM climate simulations (Liang and Wang 1997), it has not been directly evaluated. The CRM simulations offer an excellent opportunity for such an evaluation. Here we demonstrate a procedure how this is done using the CRM statistics. Figure 4 presents the CRM cloud frequency distribution as a function of cloud base and top heights. The calculation uses all 15-minute samples during the IOP at a 3-km horizontal resolution over the 600-km domain. Three major cloud clusters are evident as outlined by ellipses: deep clouds with the base below 5 km and the top reaching 10 km or higher; shallow clouds with cloud base below 5 km; and upper-level clouds with the base between 5 to 8 km. These types are similar to the TOGA-COARE result except for some differences in cloud base and top ranges (not shown).

To incorporate the dominant effect associated with this clustered structure, a first-order approximation can be formulated as follows. (1) GCM-grid mean cloud liquid and ice water profiles ($\bar{q}_1$, $\bar{q}_1$) are obtained by averaging over the entire domain. (2) The total cloud water profile ($q_1 = q_1 + q_1$) at each and every 3-km CRM-column is examined to search for all unbroken segment of cloud layers where q_t is larger than a threshold (10^{-5} g/g). (3) If a segment has its base below 4.5 km and top above 11.5 km, it is first grouped into the Cc cluster; otherwise if $\bar{q}_1 > \bar{q}_1$ at the base, then the segment falls into the Ci cluster; all the remaining ones belong to the Cs cluster. Figure 5 shows the resultant cloud frequency

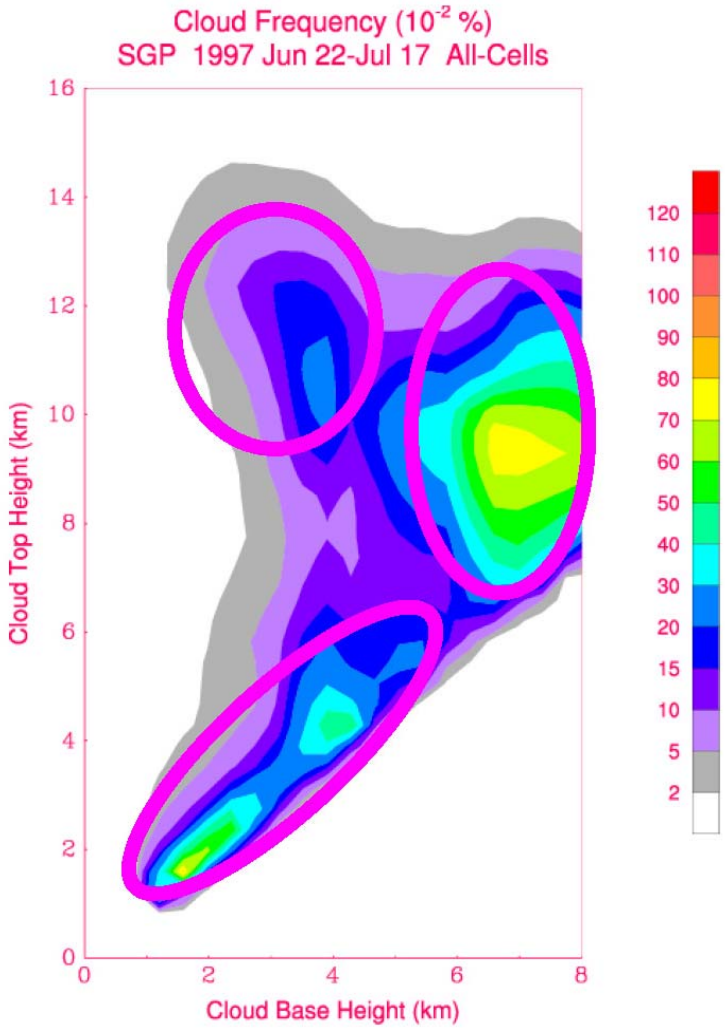

Figure 4. CRM simulated cloud frequency (10^{-4}) distribution as a function of the base and top heights. Outlined by ellipses are three major cloud clusters.

distribution for each cluster. (4) GCM-grid mean cloud cover fractions (Cc, Ci, Cs) are determined from all respective segments over the whole domain. (5) The mosaic treatment with eight subcells is finally performed once using the CRM-based GCM-grid mean profiles ($\overline{q}_1$, $\overline{q}_1$,Cc, Ci, Cs). Note that in this initial attempt, loud liquid and ice water profiles are identical for all clusters. We do distinguish the effects of cloud liquid versus ice by conserving their mass ratio over the domain. Again this liquid versus ice ratio profile is identical for all clusters. The above procedure is conducted at each time step.

Figure 6 compares surface and TOA radiative fluxes with all 15-minute samples between the CRM (M0), GCM (M1) and mosaic (MM) approaches. As discussed above, the GCM approach substantially underestimates the incoming SW (outgoing LW) radiations, especially in the medium (lower) range. The mosaic approach significantly reduce these biases, where both MM SW and LW fluxes at the surface and TOA line closely with M0 values. Figure 7 summarizes the comparison between ARM observations, CRM simulations, GCM and mosaic calculations in terms of means and standard

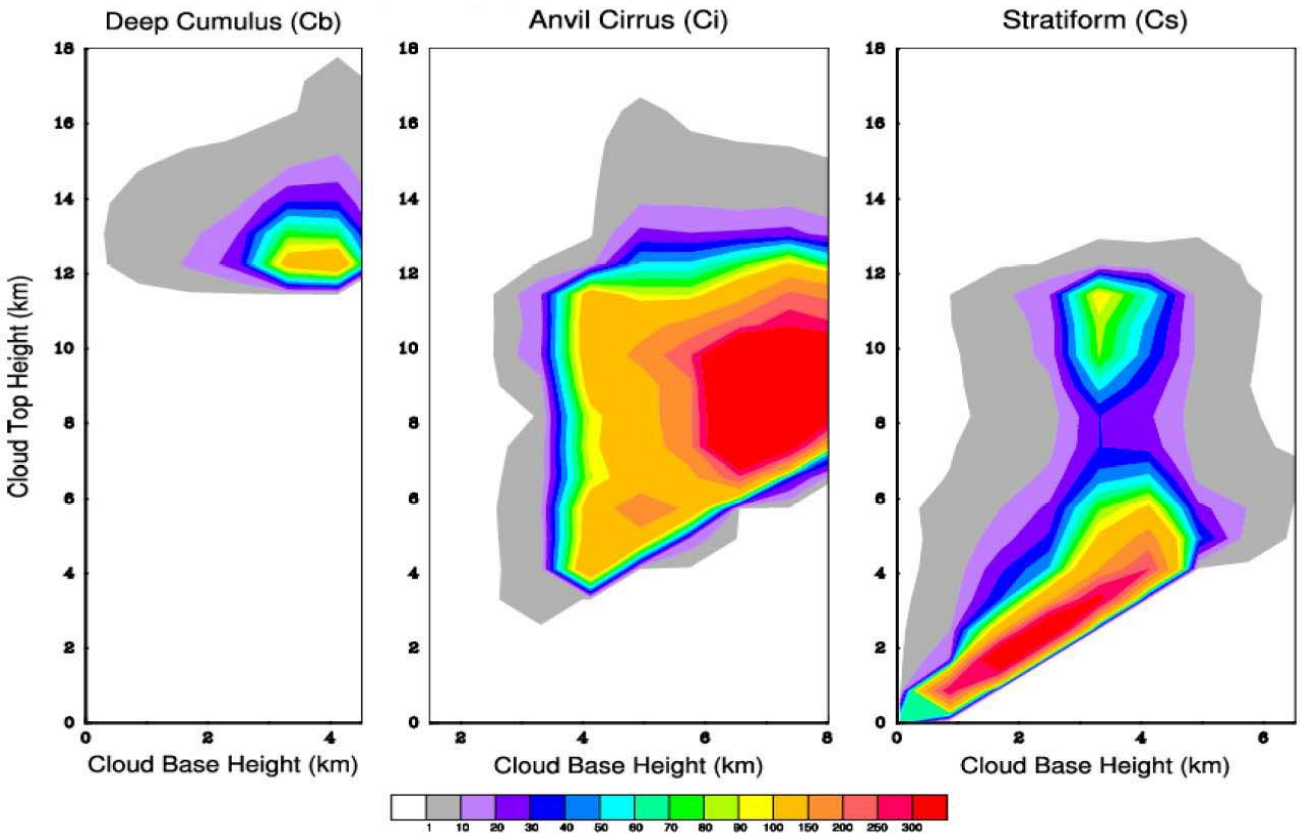

Figure 5. CRM simulated cloud frequency (10^{-5}) distribution as a function of the base and top heights for deep cumulus (Cb or convective Cc), anvil cirrus (Ci) and stratiform (Cs) clouds, approximately corresponding to the three clusters outlined by ellipses in Figure 4.

deviations of daily averages during the entire IOP. Clearly the CRM faithfully simulates the observations in both means and deviations of surface and TOA fluxes, all within measurement uncertainties. The mosaic approach accurately reproduces all these CRM statistics, with differences well within ±10 W/m^2. On the other hand, the GCM approach produces smaller incoming SW (outgoing LW) radiation by 30 (20) W/m^2 at TOA and 27 (9) W/m^2. These mean errors are accompanied by substantial overestimation of deviations, with an amplification factor of 2 (1.4) in SW (longwave) fluxes at both the surface and TOA.

Figure 8 compares the radiative SW heating, LW cooling, and total rate profiles between the CRM, GCM, and mosaic approaches. As expected, small differences occur above 12 km where little cloud presents. As compared with the CRM, the GCM approach generates substantially smaller (larger) SW heating, and reversely LW cooling, below (above) 6 km. The net effect is a systematic cooling in the whole troposphere. On the other hand, the mosaic approach accurately reproduces the heating/cooling/total rates below 6 km. Large differences remain in the upper troposphere, with enhanced SW heating and LW cooling rates. The net effect is an increase (decrease) in cooling rate

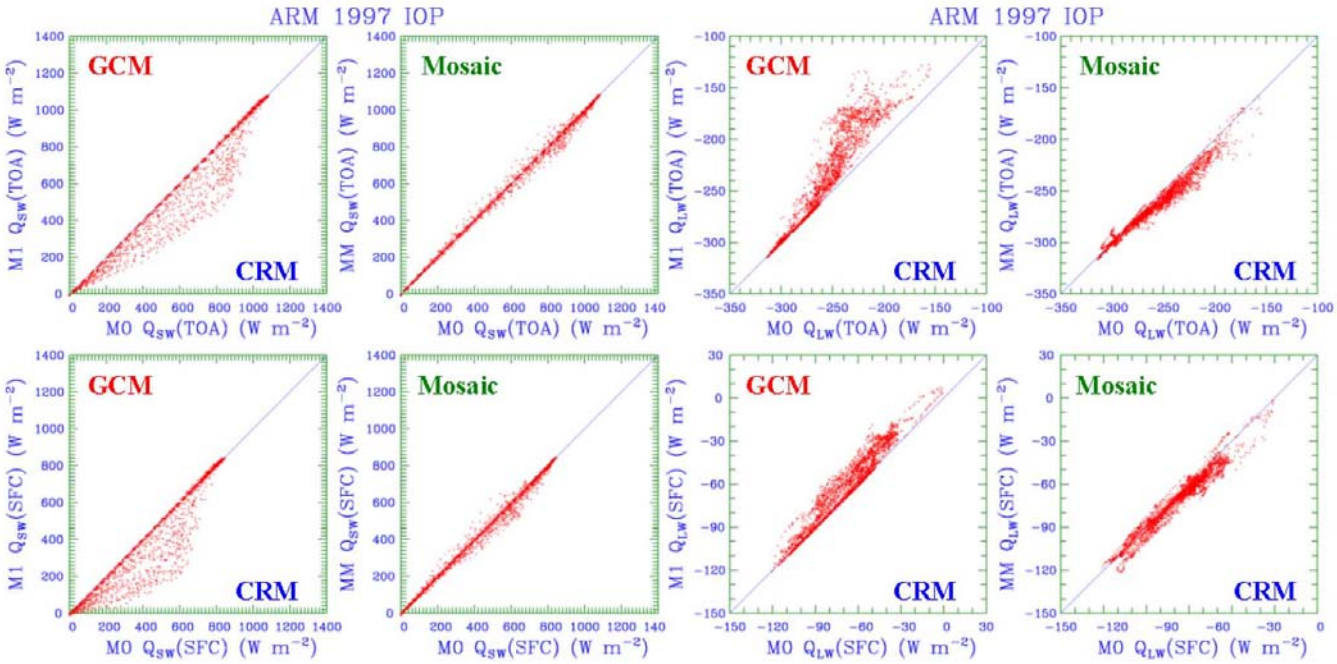

Figure 6. Scatter diagrams of GCM (M1) and mosaic (MM) versus CRM (M0) for LW (Q_{LW}) and SW (Q_{SW}) net fluxes (W m^{-2}) at the surface (SFC) and TOA. Downward fluxes are positive and all 15-minute samples are included.

between 6-8 (9-12) km. Preliminary sensitivity experiments show that these differences may result from the use of identical ($\overline{q}_1$, $\overline{q}_1$) profiles in calculation of radiative optical properties for all clusters (Cc, Ci, Cs). The work to reduce such a deficiency is in progress.

Summary

We have conducted a CRM integration during the 1997 IOP (June 22-July 17) and first evaluated it against ARM measurements. Sensitivity experiments using the CRM output were then performed to determine the relative contributions of GCM simplifications on subgrid cloud-radiation interactions. The mosaic treatment for these subgrid interactions was finally formulated from the CRM bulk cloud statistics and the result was compared with the GCM approach, using the CRM output as the reference. It has been shown that the CRM can reproduce observed radiation budgets simultaneously at TOA and surface. This success facilitates the quantification of subgrid cloud-radiation interactions, for which both cloud inhomogeneity and geometry effects are equally important. The mosaic approach with the CRM cloud statistics accurately simulates the CRM radiative budgets, and thus provides a cost-effective solution to incorporate cloud geometry and inhomogeneity effects into a GCM radiation parameterization. An accurate implementation of the mosaic approach, however, requires a realistic GCM prediction of cloud macrogrouping (CC, Ci, Cs fractions) and inhomogeneity (liquid, ice mean, and variances).

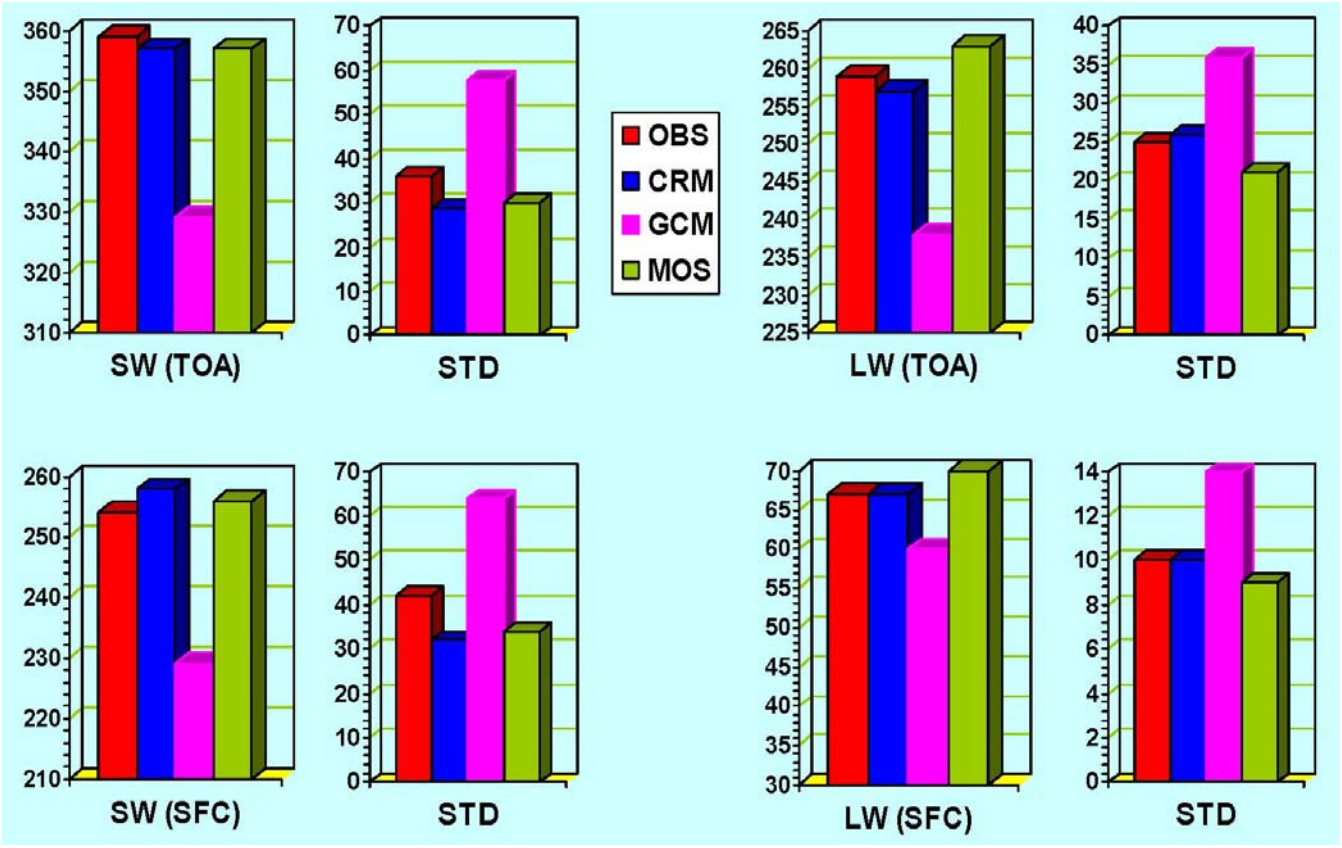

Figure 7. Means and standard deviations (STD) of daily averages from observations (OBS), CRM simulations, GCM and mosaic (MOS) calculation for upward LW and downward SW net fluxes (W m^{-2}) at the surface (SFC) and TOA.

Acknowledgements

We thank numerous ARM science team members for making various ARM data available to us. This research is supported by the Office of Science (BER), U.S. Department of Energy, Grant No. DE-FG02-02ER63483.

Corresponding Author

Xiaoqing Wu, wuxq@iastate.eedu, (515) 294-9872

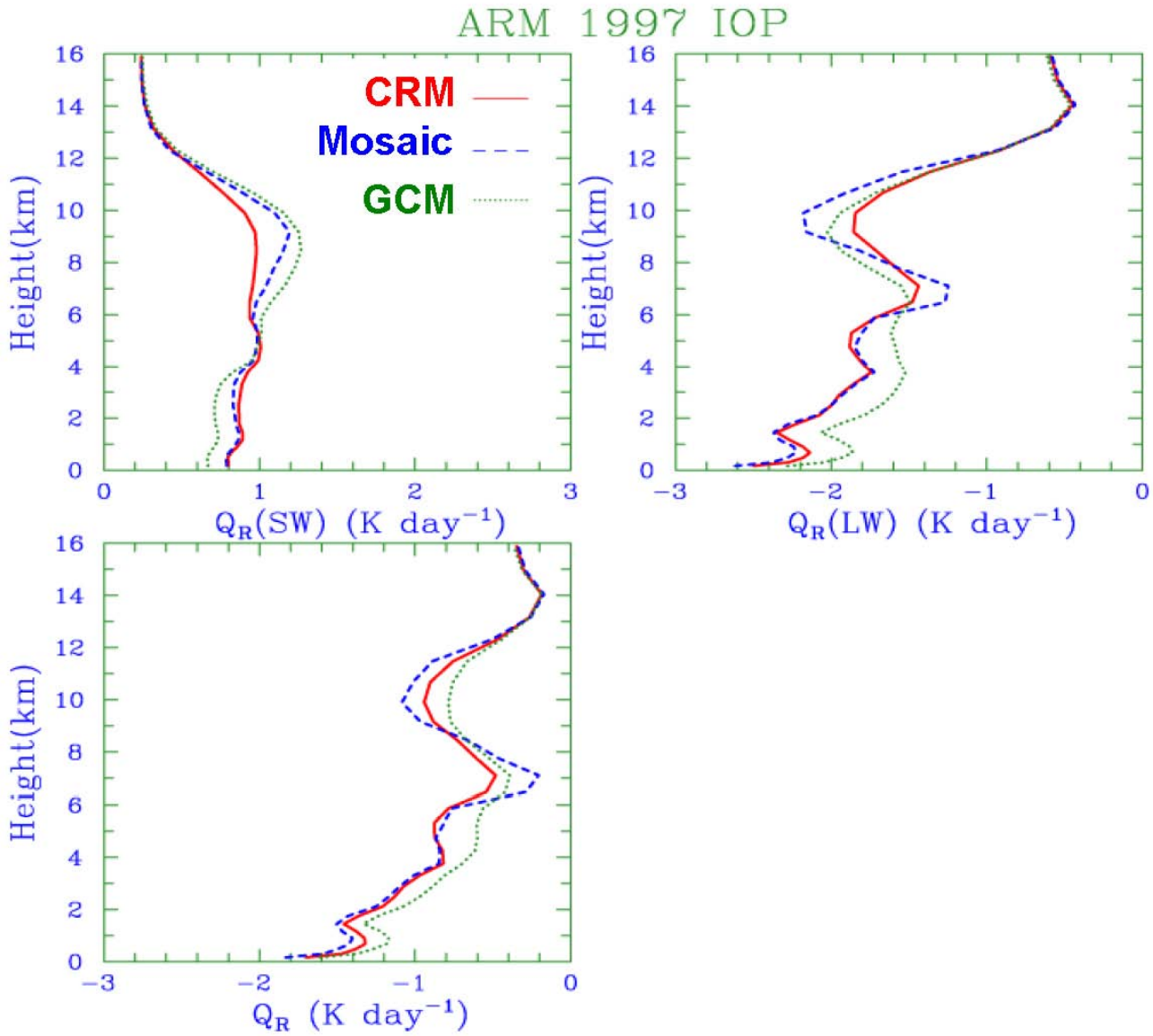

Figure 8. Domain mean LW, SW and total heating/cooling rate (Q_R: K day^{-1}) profiles as simulated by the CRM and calculated by the GCM and mosaic approaches, averaged over the entire IOP.

References

Clark, T. L., W. D. Hall, and J. L. Coen, 1996: "Source Code Documentation for the Clark-Hall Cloud-Scale Model: Code Version G3CH01." NCAR Technical Note, NCAR/TN-426+STR., p. 137. (Available from NCAR Information Service, P.O. Box 3000, Boulder, Colorado 80307).

Grabowski, W. W., X. Wu, and M. W. Moncrieff, 1996: Cloud resolving modeling of tropical cloud systems during Phase III of GATE. Part I: Two-Dimensional Experiments. *J. Atmos. Sci.*, **53**, 3684-3709.

Kiehl, J. T., J. J. Hack, G. B. Bonan, B. A. Boville, B. P. Briegleb, D. L. Williamson, and P. J. Rasch, 1996: "Description of the NCAR Community Climate Model (CCM3)." NCAR Tech. Note, NCAR/TN420+STR, p. 152. (Available from NCAR Information Service, P.O. Box 3000, Boulder, Colorado 80307.)

Li, Z., H. G. Leighton, K. Masuda, and T. Takashima, 1993: Estimation of SW flux absorbed at the surface from TOA reflected flux. *J. Climate*, **6**, 317-330.

Liang, X.-Z., and W.-C. Wang, 1997: Cloud overlap effect on general circulation model climate simulations. *J. Geophys. Res.*, **102**, 11,039-11,047.

Wu, X., and X.-Z. Liang, 2003: Month-long 2D cloud-resolving model simulation and resultant statistics of cloud systems over the ARM SGP. *Proceedings of the Thirteenth Atmospheric Radiation Measurement (ARM) Science Team Meeting*, Broomfield, CO, March 3-April 4, pp. 1-11.

Wu, X., and M. W. Moncrieff, 2001: Long-term behavior of cloud systems in TOGA COARE and their interactions with radiative and surface processes. Part III: Effects on the Energy Budget and SST. *J. Atmos. Sci*., **58**, 1155-1168.

Wu, X., W. D. Hall, W. W. Grabowski, M. W. Moncrieff, W. D. Collins, and J. T. Kiehl, 1999: Long-term behavior of cloud systems in TOGA COARE and their interactions with radiative and surface processes. Part II: Effects of Ice Microphysics on Cloud-Radiation Interaction. *J. Atmos. Sci*., **56**, 3177-3195.

Zhang, M. H., and J. L. Lin, 1997: Constrained variational analysis of sounding data based on column-integrated conservations of mass, heat, moisture, and momentum: Approach and Application to ARM Measurements. *J. Atmos. Sci*., **54**, 1503-1524.